

# A Stochastic Approach to Examining the Seasonal Predictability of Arctic Sea Ice

Anna FitzMaurice

October 15, 2015

## 1 Introduction

### 1.1 Motivation

In the context of a warming climate, a key question of interest is the fate of the Arctic sea ice. Reductions in the sea ice extent have the potential to greatly affect Arctic communities and ecosystems, and an ice-free Arctic would have a range of commercial and geopolitical implications related to the opening of previously unnavigable shipping routes. More fundamentally, the Arctic sea ice is often viewed as a diagnostic for the state of the warming Earth system, and its decline is one of the most striking indicators of modern climate change. While it is apparent that with sufficient warming the sea ice will eventually all be lost in the Arctic, the specifics of this decline are less well understood. This is related to the fact that superposed on the clear seasonal cycle and general decreasing trend displayed in the satellite record of the Arctic sea ice extent (shown in Figure 1) is significant variability on the annual timescale.

The seasonal growth and decline of Arctic sea ice is tied to the large variations in insolation at high latitudes over the course of the year. During the winter when the daylight hours are short or non-existent, the Arctic ocean cools sufficiently to allow ice to form, attaining its maximum extent in March. As the daylight hours increase through spring and summer, the Arctic warms and the ice melts back to reach its minimum extent in early September. The variability observed on top of this seasonal cycle is in part due to the interannual variability of the underlying climate, but also central to this variability is the existence of strong feedbacks in the sea ice system. Positive feedbacks act to magnify the effect of any small perturbation to the sea ice extent, while negative feedbacks dampen perturbations. It is consequently not just the underlying climate variability that complicates seasonal prediction, but also fluctuations in the strength of these feedbacks on different timescales.

Due to the intrinsic sensitivity of the sea ice system to perturbations, the ability of modern Global Climate Models (GCMs) to predict the Arctic sea ice extent seasonally is limited. In this project, it is hoped that insight might be gained by application of stochastic theory to an idealized sea ice model, which captures the essential physics of the sea ice system while allowing for unmodelled variability by inclusion of a noise term. The physical understanding derived from this study has implications for the interpretation of

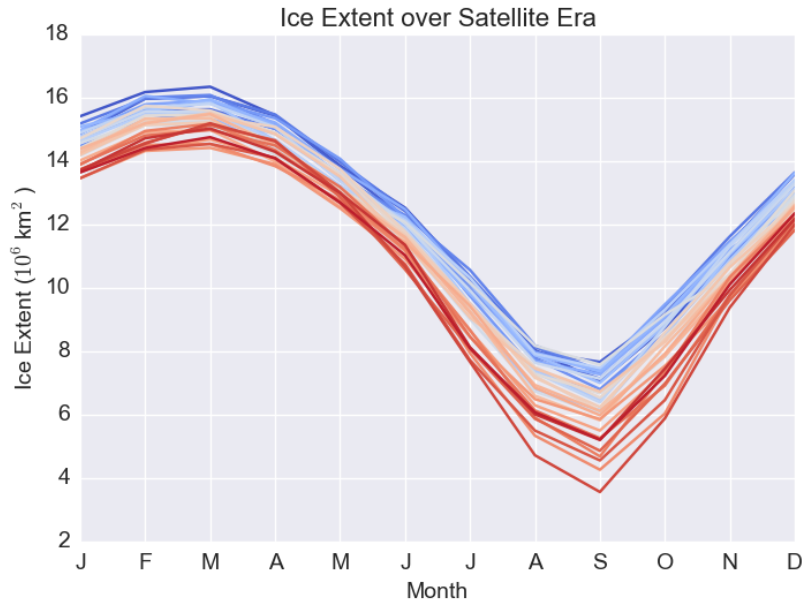


Figure 1: Area extent of Arctic sea ice since the beginning of the satellite era. Earlier years are shown in cold colors, with later years in warmer colors. In addition to the general decreasing trend over the satellite era, there is interannual noise in the ice extent, with a maximum variability displayed in September. (Data Source: NSIDC)

GCM results concerning short term Arctic sea ice prediction, and helps identify the key processes GCMs must capture if they are to be successful at seasonal forecasting.

## 1.2 Defining predictability

Predictability describes our ability to say something about the state of a system at some future time, given a specific initial condition. Mathematically, there are several ways to quantify what is intuitively understood by predictability. A measure frequently used to make statements about the predictability of Arctic sea ice is the correlation coefficient between sea ice anomalies at a given start month and subsequent months of increasing lag time, as shown for the sea ice extent data from the satellite era in Figure 2A. The decrease in the correlation coefficient with increasing lag is associated with a decline in predictability. However, how the time variation of the correlation coefficient relates to a stochastic interpretation of the system is not immediately obvious. Instead, a more transparent measure of predictability is the standard deviation of anomaly trajectories for a given point in time: if the standard deviation increases from a given start month to a later month, we might expect predictability to decrease due to the divergence of trajectories from nearby initial conditions. On the other hand, if the standard deviation decreases over the forecast period, the convergence of trajectories might be associated with an increase in predictability.

The standard deviation of the ice anomaly (once the seasonal cycle is removed) for the

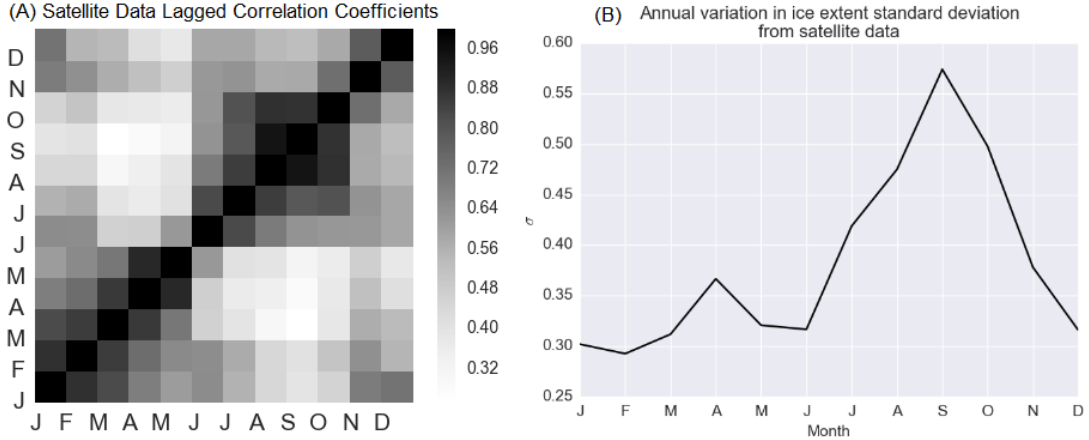


Figure 2: Two measures of predictability for the detrended Arctic sea ice extent satellite data: (A) lagged correlation coefficients, and (B) path standard deviation. (Data Source: NSIDC)

detrended sea ice extent satellite data is plotted in Figure 2B. The standard deviation is seen to increase throughout the year from a winter minimum, to a maximum that coincides with the sea ice minimum in September. This suggests poor predictability of the summer minimum of Arctic sea ice in winter due to the divergence of nearby trajectories going from March to September associated with the increase in standard deviation over this time. In turn, this begs the question of whether a spring “predictability barrier” might exist for the Arctic sea ice, similar to that discussed in the literature for El Niño prediction.

### 1.3 Model skill

The stochastic interpretation of predictability is closely related to the concept of skill, defined in the modeling community as

$$\text{skill} \equiv 1 - \frac{\sigma_{\text{sim}}^2}{\sigma_{\text{ref}}^2}, \quad (1)$$

where  $\sigma_{\text{ref}}$  is the reference standard deviation of anomalies for a given period, calculated from a long control run, and  $\sigma_{\text{sim}}$  is the standard deviation of runs from a given initial condition. If the initial value problem yields the same variance as the reference, the model has no skill. As the variance of the initialized model ensemble decreases relative to the reference standard deviation, the model’s skill is said to increase.

In what follows, we use stochastic theory applied to a simple model of Arctic sea ice to explain the physical origins of variations in the predictability of Arctic sea ice, and to better understand the concept of skill. In Section 2 the simple model is introduced, and the key features of its deterministic solutions explained. Section 3 treats the application of stochastic theory to this model, and finally Section 4 considers the use of GCMs for seasonal prediction in light of the findings of the previous section.

## 2 A Simple Model for Arctic Sea Ice

### 2.1 Model description

By working with a simple model of the Arctic sea ice, it is hoped that the fundamental features of the system that act to control the annual variations in predictability might be deduced. The energy balance model of Eisenman & Wettlaufer (2009) [1] (hereon E&W09) is appropriate for this purpose in that it captures the essential physics of the Arctic sea ice, without additional complications. The model is based on a simplified version of the thermodynamic model of [3] coupled to a two-stream model of the atmosphere, which feels a heat flux convergence that depends on the meridional temperature gradient.

The model evolves the single variable  $E$ , which describes the latent heat of the sea ice or the heat content of the ocean mixed layer, depending on whether the water is frozen or not. In the case that ice is present,  $E$  is determined from the latent heat of freezing  $L_i$  times the ice thickness  $h_i$ , while in the ice-free case  $E$  is the product of the ocean heat capacity  $c_{ml}$ , the mixed layer depth  $H_{ml}$  (assumed constant), and the ocean temperature  $T_{ml}$ . Hence,

$$E \equiv \begin{cases} -L_i h_i & E < 0 \quad (\text{sea ice}) \\ c_{ml} H_{ml} T_{ml} & E \geq 0 \quad (\text{ocean}). \end{cases} \quad (2)$$

The energy variable evolves according to equation

$$\frac{dE}{dt} = [1 - \alpha(E)] F_s(t) - F_0(t) + \Delta F_0 - F_T(t)T(t, E) + F_B + \nu_0 \mathcal{R}(-E), \quad (3)$$

where  $\alpha$  is the state-dependent albedo,  $F_B$  is the oceanic heat flux to the base of the ice, and  $\mathcal{R}$  is the ramp function defined such that  $\nu_0 \mathcal{R}(-E)$  represents a constant export of 10% year<sup>-1</sup> of the sea ice in the case with ice, and is zero otherwise. The terms  $F_0 + F_T T$  are the linearization of the Stephan-Boltzmann equation for the emission of longwave radiation about freezing temperature  $T_{Fr}$  (adapted to include the dependence of the atmospheric heat flux on the meridional temperature gradient, and to allow the atmosphere to be partially opaque), and  $\Delta F_0$  is an adjustable parameter used to apply radiative forcing perturbations to the model (to mimic increased atmospheric CO<sub>2</sub> levels, for instance). For given  $F_s, F_0, \Delta F_0, F_T$ , and  $F_B$ , to close the equations it remains to specify functional forms for  $\alpha$  and  $T$ .

The albedo of solid ice  $\alpha_i$  is very high compared to the substantially lower albedo of open water  $\alpha_{ml}$ . As sea ice melts, pools of meltwater appear on the surface, leads open up, and the ice thins and eventually disintegrates. This is modelled in E&W09 by allowing the albedo to decrease smoothly from  $\alpha_i$  to  $\alpha_{ml}$  via

$$\alpha(E) = \frac{1}{2}(\alpha_{ml} + \alpha_i) + \frac{1}{2}(\alpha_{ml} - \alpha_i) \tanh\left(\frac{E}{L_i h_\alpha}\right), \quad (4)$$

for thickness parameter  $h_\alpha$ .

The surface temperature is given by

$$T(t, E) = \begin{cases} -\mathcal{R}\left[\frac{(1-\alpha_i)F_s(t)-F_0(t)+\Delta F_0}{k_i L_i/E-F_T(t)}\right] & E < 0 \\ \frac{E}{c_{ml} H_{ml}} & E \geq 0, \end{cases} \quad (5)$$

which expresses the energy balance in the three possible cases of an ice layer that is below freezing, melting ice, and an ice-free ocean. If the ice is below the freezing point,  $E$  and  $T$  are negative and ice growth occurs until a balance is reached between the surface radiative fluxes and the upward heat flux in the ice. For ice at the freezing point, ablation may occur and release latent heat, thinning the ice. These two regimes are expressed by the ramp function in equation 5. When all the ice is melted, so  $E \geq 0$ , the mixed layer is able to absorb energy and raise its temperature (dependent on the mixed layer heat capacity  $c_{ml}$  and depth  $H_{ml}$ ) to maintain radiative equilibrium.

## 2.2 Behavior of the deterministic model

For a sufficiently low forcing  $\Delta F_0$ , integration of the deterministic model yields a solution with perennial sea ice, while for high  $\Delta F_0$ , an ice-free state results. In between, E&W09 find a stable seasonally ice-free state in the full nonlinear model, but show that this solution is unstable in a partially linearized version of the model. Historically it has been proposed that seasonal ice states must be unstable due to the ice-albedo feedback, which is always positive. This has led to concerns regarding a “tipping point” in the stability of the Arctic sea ice, due to the possibility of hysteresis in the bifurcation diagram of such a system. However, in the nonlinear model E&W09 find that competing longwave effects, which allow thin ice to grow more quickly than thick ice, act to stabilize seasonal sea ice solutions. The underlying structure of the system is still the same though, and additional heating once this seasonally stable ice state has been reached could result in hysteresis behavior as the system jumps to the permanently ice-free state.

A minimal model for a seasonally stable ice cover is analyzed in [4], in which it is deduced that the minimal condition for stability of a seasonal ice state is that the seasonal cycle be broken into more than two periods such that there may be heat loss by the ocean during the period when the summer is ice-free. This follows intuitively from the understanding that the ocean mixed layer must lose its accumulated heat before ice can form.

## 3 Stochastic Theory & its Implications for Predictability

While the deterministic E&W09 model captures the essence of the seasonal cycle of Arctic sea ice, it was seen in the satellite data in Figure 1 that the real ice extent is subject to small amplitude variability superposed on this cycle. To simulate this variability, a noise term may be added to the governing ODE of the deterministic model, turning it into the Stochastic Differential Equation (SDE)

$$\frac{dE}{dt} = f(E, t) + \sigma\xi, \quad (6)$$

where the term  $f(E, t)$  encapsulates all the right-hand side forcings of Equation 3.

### 3.1 Stochastic perturbation theory

The small magnitude of the noise in the sea ice extent in relation to the amplitude of its seasonal cycle motivates the application of the stochastic perturbation theory developed by

Moon & Wettlaufer (2013) [5], in which the solution to the SDE is sought as a perturbation about the time-dependent ODE solution in terms of small parameter  $\sigma$ , which is the noise magnitude.

Starting from the deterministic equation

$$\frac{dE_s}{dt} = f(E_s, t), \quad (7)$$

we suppose that the SDE

$$\frac{dE}{dt} = f(E, t) + \sigma\xi \quad (8)$$

is solved by  $E = E_s + \eta(t)$ , for  $\eta$  small, so that the right-hand side of Equation 8 may be expanded about ODE solution  $E_s$  as

$$\frac{d\eta}{dt} \approx \left[ \left. \frac{\partial f}{\partial E} \right|_{E_s} \eta + \frac{1}{2} \left. \frac{\partial^2 f}{\partial E^2} \right|_{E_s} \eta^2 + \dots \right] + \sigma\xi \quad (9)$$

$$= c(t)\eta + d(t)\eta^2 + \sigma\xi, \quad (10)$$

where time-dependent parameters  $c$  and  $d$  are defined such that  $c(t) \equiv \partial_E f|_{E_s}$  and  $d(t) \equiv \partial_{E^2}^2 f|_{E_s}/2$ .

It follows from the above that the time evolution of perturbations to the underlying seasonal cycle of the zero-dimensional sea ice model are entirely governed at leading order by the parameters  $c$  and  $d$ . These parameters vary over the course of the year, and display a seasonal cycle just like the sea ice. Over short time periods for which perturbations remain small and the above theory is valid,  $c$  and  $d$  may be considered constant to simplify analysis. In what follows, a consideration of the system's behaviour for constant  $c$  and  $d$  of different signs will allow the roles played by  $c$  and  $d$  in determining the evolution of perturbations to the sea ice, and their resultant impact on the predictability of the system, to be understood.

### 3.2 Numerical solution

To integrate Equation 10, the Euler-Maruyama method may be employed. The Euler-Maruyama method is an adaptation of the Euler method for SDEs. At each timestep in the standard Euler integration, a Gaussian random variable is drawn from normal distribution of mean zero and standard deviation 1. This value is scaled by the size of the timestep and the noise amplitude, and added to account for the noise term in the SDE. Explicitly

$$\eta_{t+1} = \eta_t + f(\eta_t)dt + \sigma dW, \quad (11)$$

where  $dW \sim N(0, \sqrt{dt})$ . If an ensemble of such integrations are run for a given initial condition, each with different realisations of the Gaussian noise term at each timestep, a pdf of the solution may be obtained from the spread of the ensemble at a given time. This method is explained in full in [2].

Ensembles of integrations from a given small initial perturbation for constant  $c$  and  $d$  are shown in Figure 3. For different signs of  $c$ , very different behaviour is observed, with the divergence of trajectories for  $c > 0$ , and convergence for  $c < 0$ . To understand this behaviour, and the importance of the values of  $c$  and  $d$ , an analytical solution is sought.

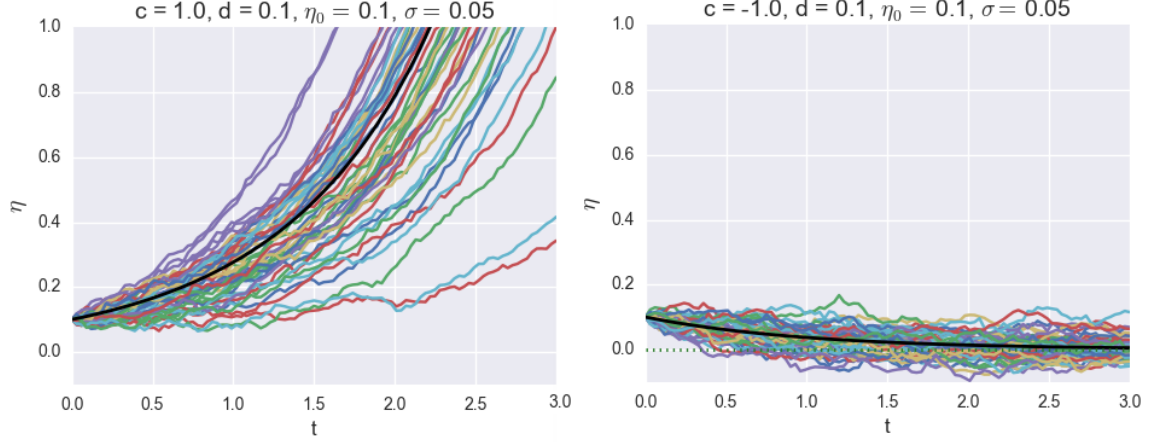


Figure 3: Realisations of integrations of Equation 10 using the Euler-Maruyama method for  $c > 0$  (left) and  $c < 0$  (right). The ensemble mean is shown in black.

### 3.3 Analytical solution

Expanding  $\eta$  in powers of the (small) noise magnitude  $\sigma$  as  $\eta = \eta_0 + \sigma\eta_1 + \sigma^2\eta_2 + \dots$ , and considering the equation at subsequent orders of  $\sigma$ ,

$$\begin{aligned}
 O(1) : \quad \frac{d\eta_0}{dt} &= c(t)\eta_0 + d(t)\eta_0^2 \\
 O(\sigma) : \quad \frac{d\eta_1}{dt} &= [c(t) + 2d(t)\eta_0(t)]\eta_1 + \xi \\
 O(\sigma^2) : \quad \frac{d\eta_2}{dt} &= [c(t) + 2d(t)\eta_0(t)]\eta_2 + d(t)\eta_1(t)^2, \\
 &\vdots
 \end{aligned} \tag{12}$$

It is immediate that the equation is deterministic at leading order, with solution

$$\eta_0 = \frac{c\eta_0(0)e^{ct}}{c + d\eta_0(0) - d\eta_0(0)e^{ct}}, \tag{13}$$

whose evolution is described by potential  $V(t) \equiv -\frac{1}{2}c\eta_0^2 - \frac{1}{3}d\eta_0^3$ . The shape of this potential for the different sign cases is shown in Figure 4. As we supposed  $\eta$  is a small perturbation to the deterministic solution and so close to zero, the salient point to take from Figure 4 is that zero is a steady state for  $c < 0$ , and an unsteady state for  $c > 0$ . In this respect  $c$  determines the stability of the system, explaining the divergence seen in the numerical solution for  $c > 0$ , and the convergence for  $c < 0$ . The parameter  $d$ , meanwhile, controls the concavity of the potential, and influences the asymmetry of the response to positive versus negative perturbations.

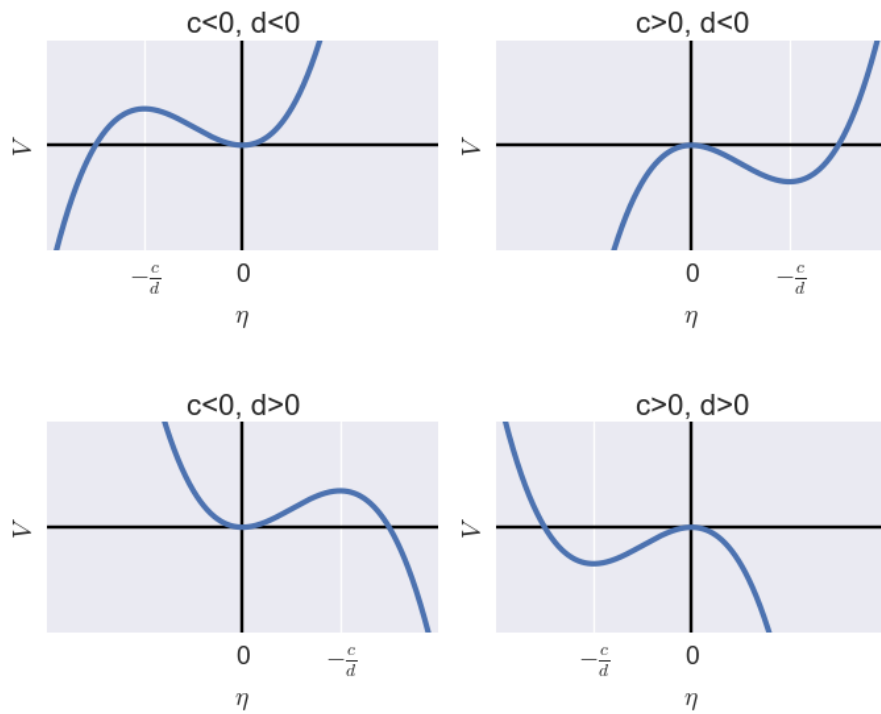


Figure 4: A schematic of the potential governing the evolution of the deterministic first order solution to the SDE.

### 3.3.1 Order $\sigma$

The stochastic term  $\xi$  enters the equation at first order in  $\sigma$ , so it is possible to write down the Fokker-Planck equation for the evolution of the pdf  $\rho$  of  $\eta_1$  for a given initial condition:

$$\frac{\partial \rho}{\partial t} = -[c(t) + 2d(t)\eta_0(t)] \frac{\partial}{\partial \eta_1} (\eta_1 \rho) + \frac{1}{2} \frac{\partial^2 \rho}{\partial \eta_1^2}. \quad (14)$$

This equation is complicated by the fact that the  $O(\sigma)$  equation is non-autonomous, due to  $c, d$ , and  $\eta_0$  being time-dependent. To solve, the Fourier transform in  $\eta_1$  is taken to give

$$\frac{\partial \hat{\rho}}{\partial t} = \tilde{c}k \frac{\partial \hat{\rho}}{\partial k} - \frac{k^2}{2} \hat{\rho}, \quad (15)$$

where  $\tilde{c}(t) \equiv c(t) + 2d(t)\eta_0(t)$ . The characteristic equations for this PDE are

$$\frac{dk}{dt} = -\tilde{c}k \quad (16)$$

$$\frac{d\hat{\rho}}{dt} = -\frac{k^2}{2} \hat{\rho}, \quad (17)$$

which integrate to give

$$k = k_0 \exp\left(-\int_0^t \tilde{c}(s) ds\right) \quad (18)$$

$$\hat{\rho} = \exp\left(-\int_0^t \frac{k^2}{2} ds\right). \quad (19)$$

Substituting for  $k$  in the equation for  $\hat{\rho}$ , taking  $k_0$  outside of the integral and then substituting back using  $k_0 = k \exp\left(\int_0^t \tilde{c}(s) ds\right)$ ,  $\hat{\rho}$  is found to be

$$\hat{\rho} = \exp\left[-\frac{k^2}{2} \left(e^{2\int_0^t \tilde{c}(s) ds} \int_0^t e^{-2\int_0^s \tilde{c}(r) dr} ds\right)\right]. \quad (20)$$

Finally, on inverting the Fourier transform we have

$$\rho = \frac{1}{\sqrt{2\pi}\sigma_T} \exp\left(-\frac{\eta_1^2}{2\sigma_T^2}\right), \quad (21)$$

where the time-evolving standard deviation  $\sigma_T^2$  is described by

$$\sigma_T^2 = e^{2I(t)} \int_0^t e^{-2I(s)} ds, \quad (22)$$

$$I(t) = \int_0^t [c(s) + 2d(s)\eta_0(s)] ds. \quad (23)$$

From this it can be deduced that the standard deviation, and hence the predictability, of perturbation trajectory ensembles is dependent on the parameters  $c$  and  $d$ . For negative  $c$  there is the possibility that the standard deviation will converge with time, and hence a

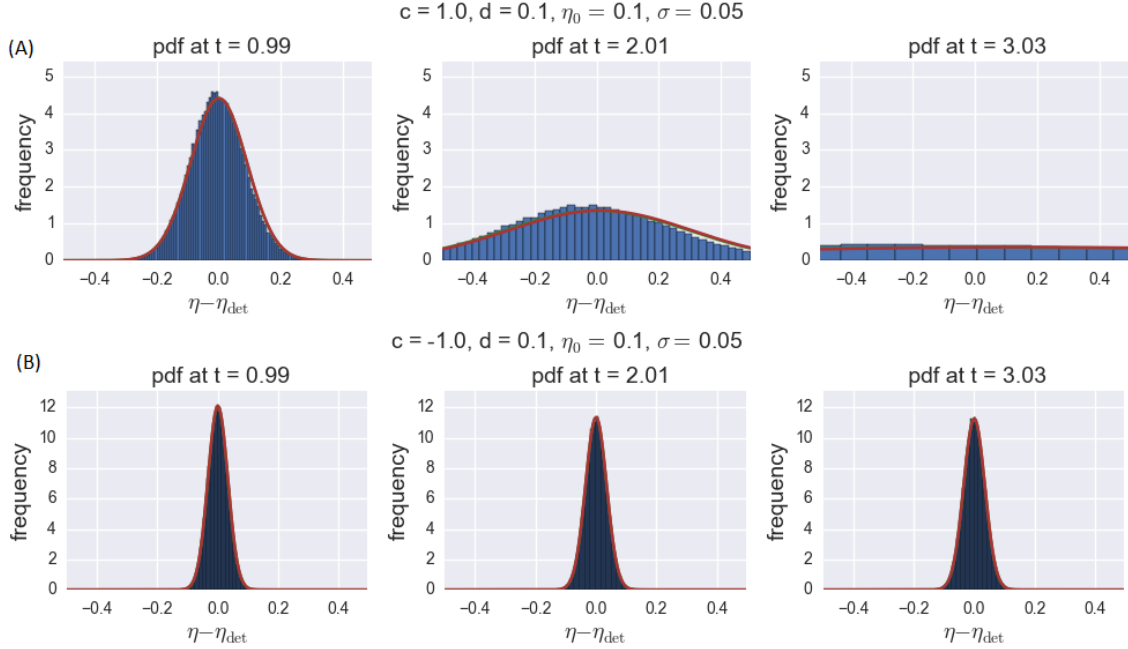


Figure 5: Left to right: Time evolution of the pdf of a perturbation  $\eta$  once its deterministic  $O(1)$  part has been subtracted for (A)  $c > 0$  and (B)  $c < 0$  ( $c, d$  constant). Numerical integrations are shown in the blue histograms, and the  $O(\sigma)$  analytical solution is overlaid in red.

degree of predictability will be maintained, while for positive  $c$  it can be seen that  $\sigma_T$  will diverge, and information will be lost. This agrees with the interpretation of  $c$  as defining the stability of the system at first order, as noise is magnified when the system is in an unstable state, and damped when the system is stabilizing.

This analytical solution is compared to the pdfs computed numerically from ensemble integrations of the SDE in Figure 5. In Figure 5A, for case  $c > 0$  when the deterministic solution is close to an unstable steady state, the analytical solution agrees with the numerically observed rapid divergence of trajectories. In the stable case  $c < 0$  shown in Figure 5B, both the analytical and numerical solution display the maintenance of a tight Gaussian centred about the deterministic solution. There is some divergence in the tails between the analytical and numerical solutions for the case  $c > 0$ , but overall the agreement is fair.

The role of parameter  $d$  is explored in Figure 6, in which the time evolution of standard deviation  $\sigma_T^2$  is plotted for various sign choices of  $c$  and  $d$ . There is either exponential growth or convergence of the standard deviation, depending on the sign of  $c$ , as seen in Figure 5. The parameter  $d$  has a lower order effect on the rate of this growth or convergence.

### 3.3.2 Approximations for small perturbations at small time

To understand the influence of  $c$  and  $d$  more clearly in Equation 22, consider the evolution of a small perturbation over a short time period, so  $\epsilon \equiv d\eta_0(0) \ll 1$  and  $ct \ll 1$ . Such solutions

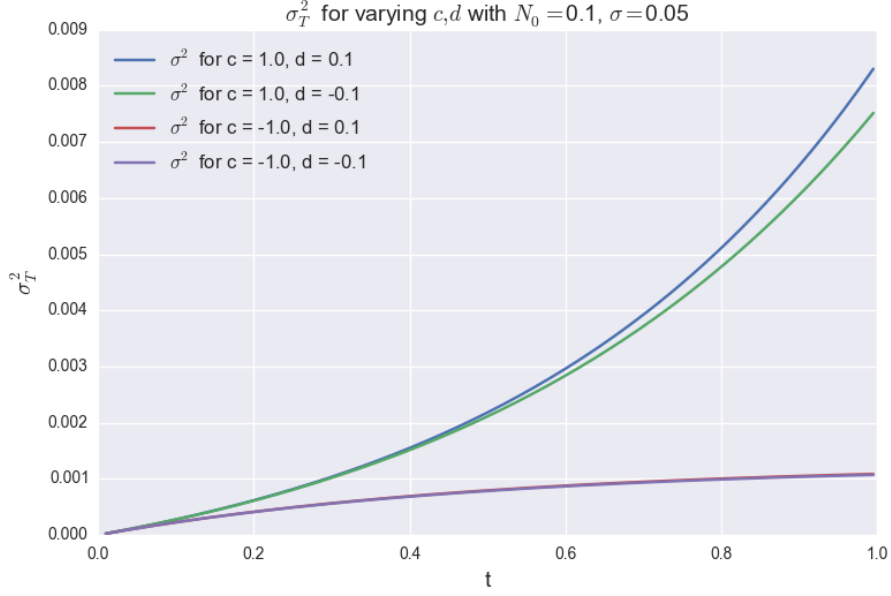


Figure 6: Time evolution of the  $O(\sigma)$  standard deviation for various constant values of  $c$  and  $d$ .

are relevant as perturbations to the Arctic sea ice are generally small in comparison to the climatological value, and the initial evolution of the stochastic solution is of most interest in determining the roles of  $c$  and  $d$ .

On introducing small parameter  $\epsilon$ , we have that by definition,

$$\tilde{c} = c + \frac{2c\epsilon e^{ct}}{c + \epsilon(1 - e^{ct})}. \quad (24)$$

So substituting into the expression for  $I(t)$ ,

$$\begin{aligned} I(t) &= ct + 2 \int_0^t \frac{c\epsilon e^{cs}}{c + \epsilon(1 - e^{cs})} ds \\ &= ct + 2 \log \left( \frac{c}{c + \epsilon(1 - e^{ct})} \right), \end{aligned} \quad (25)$$

assuming constant  $c$  and  $d$ . It follows that

$$\begin{aligned} \sigma_T^2 &= e^{2I(t)} \int_0^t e^{-2I(s)} ds \\ &= e^{2ct} \left( \frac{c}{c + \epsilon(1 - e^{ct})} \right)^4 \int_0^t e^{-2cs} \left( 1 + \frac{\epsilon}{c}(1 - e^{cs}) \right)^4 ds. \end{aligned} \quad (26)$$

Thus far, no assumptions have been made other than that  $c$  and  $d$  are constants. If it is now supposed that  $\epsilon$  is small, the binomial parts of the above expression for the standard

deviation may be expanded to give

$$\begin{aligned}
\sigma_T^2 &\simeq e^{2ct} \left(1 - \frac{4\epsilon}{c}(1 - e^{ct})\right) \int_0^t e^{-2cs} \left(1 + \frac{4\epsilon}{c}(1 - e^{cs})\right) ds \\
&= e^{2ct} \left(1 - \frac{4\epsilon}{c}(1 - e^{ct})\right) \left(\frac{1}{2c}(1 - e^{-2ct}) - \frac{2\epsilon}{c^2}(1 - e^{-ct})^2\right) \\
&= \left(1 + \frac{4\epsilon}{c}(e^{ct} - 1)\right) \left(\frac{1}{2c}(e^{2ct} - 1) - \frac{2\epsilon}{c^2}(e^{ct} - 1)^2\right). \tag{27}
\end{aligned}$$

Then to  $O(\epsilon)$ , the standard deviation becomes

$$\sigma_T^2 \simeq \frac{1}{2c}(e^{2ct} - 1) + \epsilon \frac{2}{c^2} e^{ct} (e^{ct} - 1)^2. \tag{28}$$

From this approximate expression, the role of  $c$  and  $d$  deduced from numerically integrating the full expression for the standard deviation can be seen directly. If  $c$  is negative, then the limit as  $t \rightarrow \infty$  can be found as  $-1/2c$ , whereas if  $c$  is positive, the variance grows without bound with time. The parameter  $d$  only enters in combination with the initial perturbation  $\eta_0(0)$  through  $\epsilon \equiv d\eta_0(0)$ . A positive value of  $\epsilon$  increases the growth in the variance at second order, so positive perturbations to the sea ice extent lose predictability more rapidly when  $d > 0$  than when  $d < 0$ , whereas negative perturbations lose predictability faster for  $d < 0$ .

Applying the small time limit  $ct \ll 1$ , the exponentials may be expanded to give

$$\sigma_T^2 \simeq t(1 + (2\epsilon + c)t), \tag{29}$$

demonstrating the role of both  $c$  and  $d$  (through the parameter  $\epsilon$ ) in the divergence of trajectories at small time. As discussed previously, both positive  $c$  and positive  $\epsilon$  contribute to the loss of predictability due to the increase of  $\sigma_T^2$  with time.

### 3.3.3 Order $\sigma^2$

At  $O(\sigma^2)$ , the stochasticity is no longer explicit in the  $\eta_2$  equation, but enters through the appearance of the stochastic variable  $\eta_1$ . To obtain a Fokker-Planck equation at second order then, we return to equation 10, and write down Fokker-Planck equation

$$\frac{\partial \rho}{\partial t} = -\frac{\partial}{\partial \eta}(\tilde{c}\eta + d\eta^2)\rho + \frac{\sigma^2}{2} \frac{\partial^2 \rho}{\partial \eta^2}. \tag{30}$$

Now rescaling by defining  $y$  such that  $\eta = \sigma y$ ,

$$\frac{\partial \rho}{\partial t} = -\frac{\partial}{\partial y}(\tilde{c}y + d\sigma y^2)\rho + \frac{1}{2} \frac{\partial^2 \rho}{\partial \eta^2}, \tag{31}$$

the Fokker-Planck equation may be expanded in powers of  $\sigma$  as

$$\begin{aligned}
O(1) : \quad \frac{\partial \rho_0}{\partial t} &= -\frac{\partial}{\partial y}(\tilde{c}y\rho_0) + \frac{1}{2} \frac{\partial^2 \rho_0}{\partial y^2} \\
O(\sigma) : \quad \frac{\partial \rho_1}{\partial t} &= -\frac{\partial}{\partial y}(\tilde{c}y\rho_1) + \frac{1}{2} \frac{\partial^2 \rho_1}{\partial y^2} - \frac{\partial}{\partial y}(dy^2\rho_0) \\
&\vdots
\end{aligned} \tag{32}$$

Due to the rescaling employed, the  $O(1)$  equation is identical to that seen previously in the  $O(\sigma)$  problem, and the  $O(\sigma^2)$  solution comes from the  $O(\sigma)$  Fokker-Planck equation above. Note that the form of the higher order equation is the same as that of the lower order equation, but with an additional forcing term determined by the lower order solution.

To solve, a Fourier transform is taken in  $y$  to give

$$\frac{\partial \hat{\rho}_1}{\partial t} = \tilde{c}k \frac{\partial \hat{\rho}_1}{\partial k} - \frac{k^2}{2} \hat{\rho}_1 + idk \frac{\partial^2 \hat{\rho}_0}{\partial k^2}. \quad (33)$$

Substituting in the known Gaussian form of  $\hat{\rho}_0$ , the method of characteristics may be applied similarly to before to solve for  $\hat{\rho}_1$ . It is found that

$$\hat{\rho}_1 = id [S(t)k^3 - M(t)k] \exp\left(-\frac{\sigma_T^2 k^2}{2}\right), \quad (34)$$

$$\text{for: } S(t) = e^{3I(t)} \int_0^t \sigma_T^4 e^{-3I(s)} ds, \quad (35)$$

$$M(t) = e^{I(t)} \int_0^t \sigma_T^2 e^{-I(s)} ds. \quad (36)$$

Inverting for  $\rho_1$ ,

$$\rho_1 = dM(t) \frac{\partial \rho_0}{\partial y} + dS(t) \frac{\partial \rho_0}{\partial y^3}. \quad (37)$$

So recalling that  $y = \eta/\sigma$ ,

$$\rho \approx \rho_0 + \sigma \rho_1 \quad (38)$$

$$= \rho_0 + \sigma^2 dM(t) \frac{\partial \rho_0}{\partial y} + \sigma^4 dS(t) \frac{\partial^3 \rho_0}{\partial y^3} \quad (39)$$

$$= \left[1 - \frac{dM}{\sigma_T^2} \eta + \frac{dS}{\sigma_T^4} (3\eta - \eta^3)\right] \rho_0. \quad (40)$$

### 3.3.4 Evolution of moments

The analytical form of the probability distribution calculated to second order in  $\sigma$  has the following moments

$$\langle \eta \rho \rangle = -\sigma^2 dM \quad (41)$$

$$\langle \eta^2 \rho \rangle = (\sigma \sigma_T)^2 \quad (42)$$

$$\langle \eta^3 \rho \rangle = \sigma^4 (3dM \sigma_T^2 - 6dS). \quad (43)$$

The distribution skewness, defined as

$$Sk \equiv \frac{\langle \eta^3 \rho \rangle - 3 \langle \eta \rho \rangle \langle \eta^2 \rho \rangle - \langle \eta \rho \rangle^3}{\langle \eta^2 \rho \rangle^{3/2}} \quad (44)$$

can be calculated from these moments as

$$Sk = \frac{\sigma}{\sigma_T^3} \left[ -6dS + 6d\sigma_T^2 M + \sigma^2 d^3 M^3 \right]. \quad (45)$$

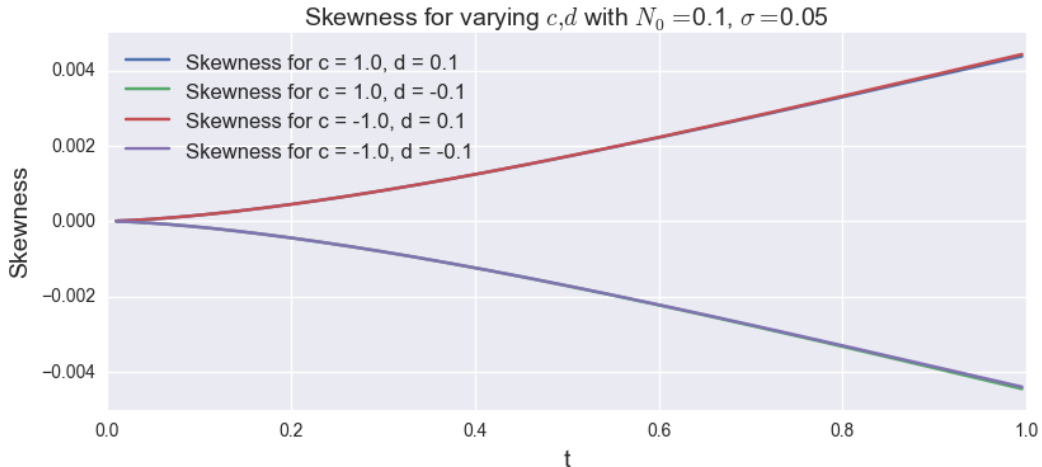


Figure 7: Evolution of the perturbation pdf skewness with time, for various constant values of parameters  $c$  and  $d$ .

This is plotted in Figure 7. Inclusion of the second order correction yields little improvement of the analytic solution, but it allows the interpretation of the parameter  $d$  as the asymmetry present in the system, when coupled with initial condition  $\eta(0)$ . For  $\eta(0)d$  positive, the skewness evolves to positive values, while for  $\eta(0)d$  negative, the skewness becomes more and more negative with time. This may be intuitively understood by referring to the potentials in Figure 4, in which it can be seen that if  $\eta(0)d$  is positive, the initial condition is on the same side as the origin as the unstable steady state, while if  $\eta(0)d$  is negative, it will be on the same side of the origin as the stable steady state. Depending on the stability of this nearby secondary fixed point, the tails of the distribution evolve differently, resulting in a positive or negative skewness.

### 3.4 Physical interpretation

From the simple model of Arctic sea ice, it has been seen that increases in the standard deviation of trajectories are caused by  $c$  positive, while convergence of trajectories is achieved for  $c$  negative. Returning to the definition of  $c$  as  $\partial_E f|_{E_S}$ ,  $c$  may be interpreted as representing feedbacks in the sea ice system. For  $c$  positive, the forcing  $f$  increases with the ice thickness variable  $E$  implying that positive feedbacks dominate, while for  $c$  negative, an increase in  $E$  causes a reduction in the ODE forcing so that the system is controlled by negative feedbacks. This interpretation allows a physical explanation for the seasonal variation of the sea ice extent standard deviation in terms of the annual variation of feedback strengths in the Arctic.

The two main relevant feedbacks in the Arctic are the ice-albedo feedback and the longwave stabilization feedback. The ice-albedo feedback refers to the effect of changes in surface albedo with ice thickness and extent. Any initial ice melt reduces the surface albedo, causing more solar radiation to be absorbed, resulting in further melting. Conversely, a positive perturbation to the ice thickness or extent increases the surface albedo so that

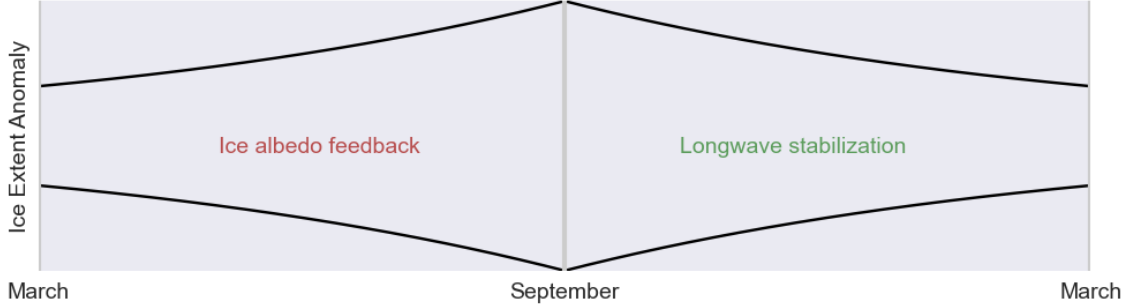


Figure 8: A schematic of the seasonal variation in trajectory standard deviation, and the physical mechanisms that control this. The spreading of trajectories in spring and summer is associated with the dominance of the positive ice-albedo feedback during this time of year, while the dominance of the negative longwave stabilization feedback in fall causes the re-focussing of trajectories going into the winter months.

more radiation is reflected, the system cools, and more ice is able to form. The ice-albedo feedback is therefore a positive feedback. The longwave stabilization feedback, on the other hand, describes the faster growth of thin ice than thick ice due to the nonlinearity of the system, and is a negative feedback. If there is a negative perturbation to the sea ice thickness, the speed at which it grows increases, pushing the system back to equilibrium. Similarly, the growth of positive perturbations is arrested, again stabilizing the system.

On a seasonal basis, the strength of the ice-albedo feedback varies in step with the solar radiation. In the winter when there is no sunlight to produce a positive ice-albedo feedback, the negative longwave stabilization feedback dominates, and we would anticipate a negative value for  $c$ . As the insolation increases through spring, the ice-albedo feedback increases in strength, raising the value of  $c$  to its summer maximum. As the value of  $c$  controls the growth of the standard deviation of trajectories, this explains the observed seasonal variation in sea ice extent standard deviation, which is low during winter and increases to a September maximum in step with the Arctic insolation levels. This situation is illustrated in the schematic in Figure 8.

The second parameter of relevance that came out of the preceding analysis was  $\epsilon$ ; the combination of  $d \equiv \partial_E^2 f|_{E_S}/2$  and  $\eta_0(0)$ . It was seen that predictability was lost more quickly in the case of positive  $\epsilon$ . The simple model shows the seasonal cycle of  $d$  as following a similar pattern to that of  $c$ ; positive in the spring and summer, and negative over winter. As  $\epsilon$  comprises both  $d$  and the sign of the initial perturbation, this suggests faster loss of predictability following anomalously high ice extents ( $\eta_0(0) > 0$ ) than for anomalously low spring ice extents ( $\eta_0(0) < 0$ ) in spring when  $d > 0$ , but the converse in fall when  $d < 0$ .

### 3.4.1 Changing predictability in a warming climate

With the aid of the physical framework outlined above, it is possible to attempt to answer the question of how the predictability of the Arctic sea ice extent might change in the context of a warming climate. Running the simple model of Eisenmann & Wettlaufer with

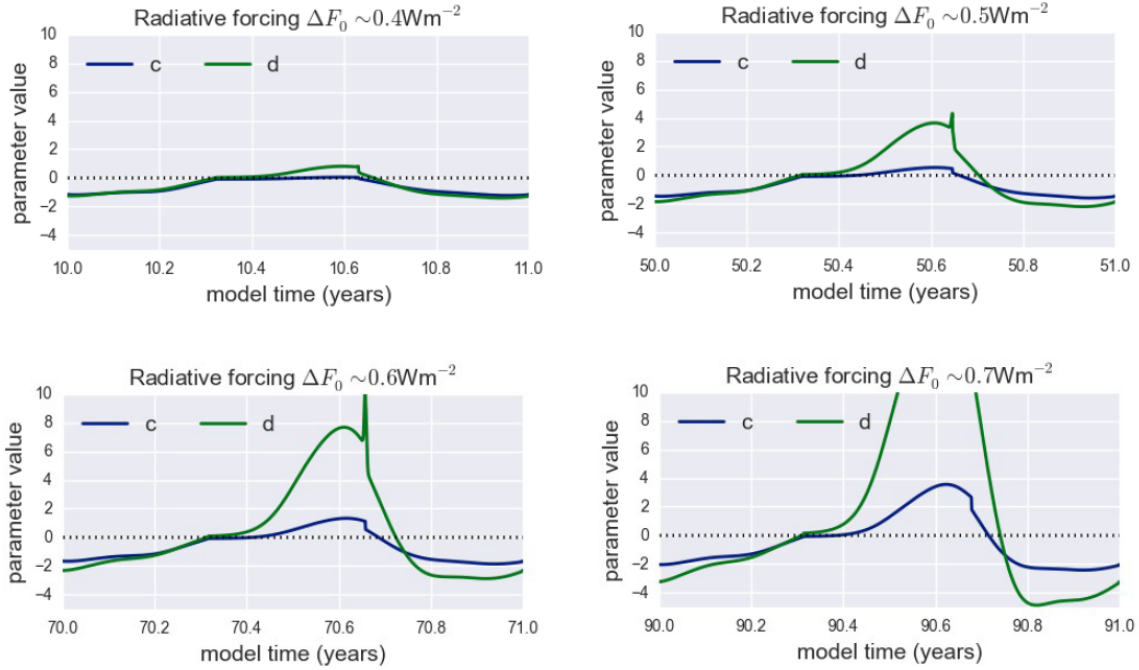


Figure 9: Steady state seasonal cycle of parameters  $c$  and  $d$  under increasing radiative forcing  $F_0$  from the E&W09 model. The seasonal cycles of both  $c$  and  $d$  are amplified as the forcing is increased from  $0.4\text{Wm}^{-2}$  to  $0.7\text{Wm}^{-2}$ .

increased values of radiative forcing  $F_0$ , the annual cycle of  $c$  is seen to amplify under global warming as shown in Figure 9. As  $c$  becomes more positive in summer months in a warmer climate, it might be anticipated that the predictability of the September minimum of Arctic sea ice will decline under global warming. Conversely, as  $c$  is seen to become more negative during winter as  $F_0$  increases, the predictability of the winter maximum might increase.

Although the influence of  $d$  on predictability is secondary to that of  $c$ , the amplification of the seasonal cycle of  $d$  could likewise contribute to a worsening predictability of summer sea ice minima following positive perturbations to the spring ice extent, but might act to improve predictability following anomalously low spring extents. Again, the converse would be true for the prediction of the winter sea ice maximum, when the sign of  $d$  is reversed.

### 3.5 The backward equation

From analysis of the Fokker-Planck equation, it has been seen that predictability in the sense of trajectory standard deviation is limited by the dominance of positive feedbacks in the sea-ice system in spring. However, given an observed sea ice extent in September, what does this feature of the system mean for our ability to pinpoint the origin of such an anomaly? This problem calls for application of the Kolmogorov Backward Equation (KBE), which gives the pdf at some initial time  $s < t_{\text{end}} \equiv 0$  of conditions that could have led to solution  $\eta_{\text{end}}$  at  $t = t_{\text{end}}$  (where stochastic perturbation is applied as before so that  $\eta$  is a small anomaly superposed on the seasonal sea ice solution).

From the  $O(\sigma)$  expansion for Equation 10, the KBE may be written down as

$$-\frac{\partial \rho}{\partial s} = [c(s) + 2d(s)\eta_0(s)]\eta_1 \frac{\partial \rho}{\partial \eta_1} + \frac{1}{2} \frac{\partial^2 \rho}{\partial \eta_1^2}. \quad (46)$$

Fourier transforming and applying the method of characteristics as for the forward equation, the standard deviation of the leading order Gaussian solution is found to be

$$\sigma_{TB}^2 = e^{-2I_B(s)} \int_s^0 e^{2I_B(r)} dr \quad (47)$$

$$I_B(s) = \int_s^0 [c(r) + 2d(r)\eta_0(r)] dr. \quad (48)$$

This is plotted backwards in time in Figure 10.

Figure 10 demonstrates that the evolution of the standard deviation of trajectories going back in time is controlled by the stability parameter  $c$  just as for forward trajectories. However, unlike for the forward case, a positive value of  $c$  leads to trajectories converging backwards in time, while a negative value of  $c$  causes them to diverge. Returning to the interpretation of  $c$  as the stability of the system, this can be understood in terms of the possible initial conditions that could have produced a given anomaly. If the system is in a stable regime ( $c < 0$ ), trajectories may have originated from a large range of ICs within the potential well, so looking back in time the pdf of ICs that could have resulted in a given anomaly is broad. On the other hand, if the system is unstable ( $c > 0$ ), there is a very low probability of the IC being far from the origin, as this is a potential hill when the system is unstable.

If the KBE standard deviation is plotted further back in time for the stable case, then the direction of the perturbation (controlled by asymmetry parameter  $\eta_0(0)d$ ) is found to matter, with some divergence in trajectories occurring if this places the perturbation on the side of the origin with a potential well, as opposed to further convergence if the perturbation was on the opposite side of the origin (see Figure 4). While this agrees with the interpretation above, its physical relevance may be limited by the fact that stochastic perturbation theory is only valid for small perturbations, as so may fail far back in time when trajectories are far from the origin.

As for the forward equations, approximations for small perturbations at small time can be made for the backward equation to see directly the role of  $c$ ,  $d$ , and  $\eta_0(0)$  in the equation. For small parameter  $\epsilon$  defined as before, for constant  $c$  and  $d$  the expression for  $I_B(s)$  is

$$\begin{aligned} I_B(t) &= ct + 2 \int_0^t \frac{c\epsilon e^{-cs}}{c + \epsilon(1 - e^{-cs})} ds \\ &= ct - 2 \log \left( \frac{c}{c + \epsilon(1 - e^{-ct})} \right), \end{aligned} \quad (49)$$

where the change of variables  $t \equiv -s$  has been made in the definition of  $I_B$  for ease of comparison with the forward equation. Then

$$\begin{aligned} \sigma_{TB}^2 &= e^{-2I_B(t)} \int_0^t e^{2I_B(s)} ds \\ &= e^{-2ct} \left( \frac{c}{c + \epsilon(1 - e^{-ct})} \right)^4 \int_0^t e^{2cs} \left( 1 + \frac{\epsilon}{c}(1 - e^{-cs}) \right)^4 ds. \end{aligned} \quad (50)$$

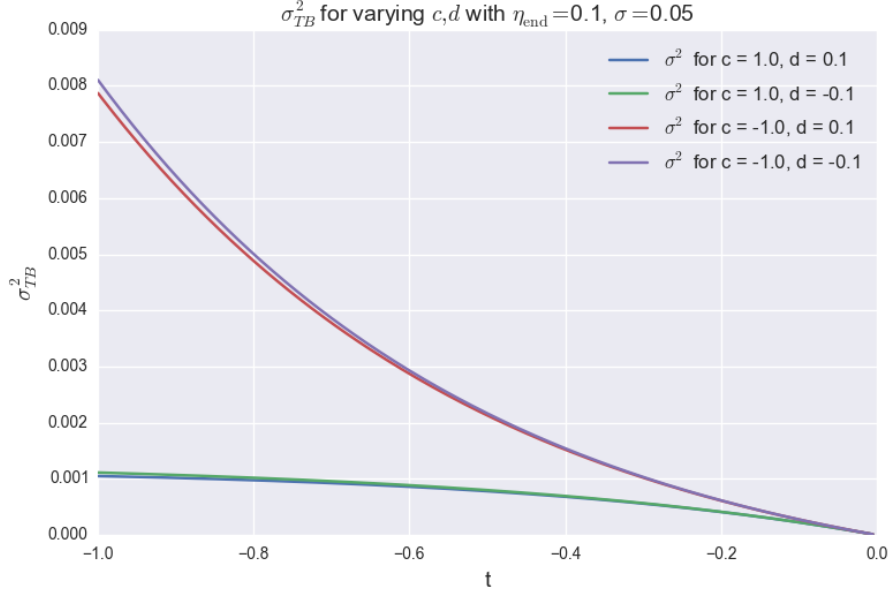


Figure 10: Trajectory standard deviation evolution backward in time, as calculated from applying the Kolmogorov Backward Equation to the  $O(\sigma)$  problem for various constant values of parameters  $c$  and  $d$ .

Now assuming that  $\epsilon$  is small, the binomials may be expanded as before, allowing integration for the approximate expression

$$\sigma_B^2 \simeq \left(1 - \frac{4\epsilon}{c}(1 - e^{-ct})\right) \left(\frac{1}{2c}(1 - e^{-2ct}) + \frac{2\epsilon}{c^2}(1 - e^{-ct})^2\right). \quad (51)$$

Then to  $O(\epsilon)$ ,

$$\sigma_{TB}^2 \simeq \frac{1}{2c}(1 - e^{-2ct}) - \frac{2\epsilon}{c^2}e^{-ct}(1 - e^{-ct})^2. \quad (52)$$

It can immediately be seen from this expression that the influence of  $c$  on the standard deviation has changed signs; now a positive value of  $c$  allows the variance to converge, while negative  $c$  leads to exponential growth of the variance with time. Similarly, the sign of  $\epsilon$  is flipped, with positive  $d\eta_0(0)$  now reducing the divergence of trajectories.

These findings bode well for the attribution of a given year's September sea ice minimum to events earlier in the season, even if the forward equation suggests that the prediction of this minimum is inherently limited. There have been attempts in the literature to trace anomalous sea ice extents in specific years to the spring melt pond fraction [6], or the occurrence of given winter storms [7]. In particular, our understanding of the role of  $\epsilon$  suggests attribution of extreme summer minima (i.e. negative  $\eta_0(0)$ ) should be easier than the attribution of maxima (positive  $\eta_0(0)$ ) when  $d$  has a positive value as in summer.

### 3.6 Understanding skill

Returning to the concept of skill defined in the Section 1.3, we may now relate this to the system's stability in a similar manner to the above treatment of predictability. Recall that

$$\text{skill} \equiv 1 - \frac{\sigma_{\text{sim}}^2}{\sigma_{\text{ref}}^2}, \quad (53)$$

for reference standard deviation  $\sigma_{\text{ref}}^2$ , and simulation standard deviation  $\sigma_{\text{sim}}^2$ . In the context of the simple model considered previously,  $\sigma_{\text{sim}}^2$  is the quantity  $\sigma_T^2$  defined in Equation ???. To calculate  $\sigma_{\text{ref}}^2$ , the long time limit of the  $O(\sigma)$  SDE is taken following [5], which gives

$$\sigma_{\text{ref}}^2 = \exp\left(2 \int_0^{\tilde{t}} c(s) ds\right) \left[ I_{\tilde{t}} + \frac{1}{e^{2\gamma} - 1} I_T \right], \quad (54)$$

where

$$I_{\tilde{t}} \equiv \int_0^{\tilde{t}} \exp\left(-2 \int_0^r c(s) ds\right) dr, \quad (55)$$

$$I_T \equiv \int_0^T \exp\left(-2 \int_0^r c(s) ds\right) dr \quad (56)$$

$$\gamma \equiv - \int_0^T c(s) ds, \quad (57)$$

for  $t = nT + \tilde{t}$ , where  $T$  is the period length of  $c$ , and  $\tilde{t} = t \bmod T$ .

To make the skill calculation numerically tractable, consider a simplified two-season model in which  $c = c_P > 0$  for six months ('spring'), and  $c = -c_N < 0$  for six months ('fall');

$$c(t) = \begin{cases} c_P & 0 \leq t < 1/2 \\ -c_N & 1/2 \leq t < 1, \end{cases} \quad (58)$$

where  $c_P$  and  $c_N$  are positive and  $c_N > c_P$  for stability. In this system,

$$\begin{aligned} I_T &= \int_0^{1/2} \exp\left(-2 \int_0^r c(s) ds\right) dr + \int_{1/2}^1 \exp\left(-2 \int_0^r c(s) ds\right) dr \\ &= \int_0^{1/2} e^{-2c_P r} dr + \int_{1/2}^1 \exp\left(-c_P + 2c_N\left(r - \frac{1}{2}\right)\right) dr \\ &= \frac{1}{2c_P} (1 - e^{-c_P}) + \frac{1}{2c_N} (e^{c_N - c_P} - e^{-c_P}). \end{aligned} \quad (59)$$

Also,

$$\begin{aligned} \gamma &= - \int_0^{1/2} c_P ds + \int_{1/2}^1 c_N ds \\ &= \frac{1}{2} (c_N - c_P). \end{aligned} \quad (60)$$

The value of  $I_{\tilde{t}}$  depends on which half of the year the model is in. When  $0 \leq \tilde{t} < 1/2$ ,

$$I_{\tilde{t}} = \int_0^{\tilde{t}} \exp(-2c_P r) dr = \frac{1}{2c_P} (1 - e^{-2c_P \tilde{t}}), \quad (61)$$

while if  $1/2 \leq \tilde{t} < 1$ ,

$$\begin{aligned} I_{\tilde{t}} &= \int_0^{1/2} \exp(-2c_P r) dr + \int_{1/2}^{\tilde{t}} \exp\left(-c_P + 2c_N\left(r - \frac{1}{2}\right)\right) dr \\ &= \frac{1}{2c_P} (1 - e^{-c_P}) + \frac{1}{2c_N} e^{-(c_P + c_N)} (e^{2c_N \tilde{t}} - e^{c_N}). \end{aligned} \quad (62)$$

The above expressions give reference standard deviation

$$\begin{aligned} \sigma_{\text{ref}}^2 &= e^{2c_P \tilde{t}} \left[ \frac{1}{2c_P} (1 - e^{-2c_P \tilde{t}}) + \right. \\ &\quad \left. \frac{1}{e^{(c_N - c_P)} - 1} \left( \frac{1}{2c_P} (1 - e^{-c_P}) + \frac{1}{2c_N} (e^{(c_N - c_P)} - e^{-c_P}) \right) \right] \end{aligned} \quad (63)$$

in the first part of the year (i.e.  $0 \leq \tilde{t} < 1/2$ ), and

$$\begin{aligned} \sigma_{\text{ref}}^2 &= e^{c_P + c_N - 2c_N \tilde{t}} \left[ \frac{1}{2c_P} (1 - e^{-c_P}) + \frac{1}{2c_N} e^{-(c_P + c_N)} (e^{2c_N \tilde{t}} - e^{c_N}) \right. \\ &\quad \left. + \frac{1}{e^{(c_N - c_P)} - 1} \left( \frac{1}{2c_P} (1 - e^{-c_P}) + \frac{1}{2c_N} (e^{(c_N - c_P)} - e^{-c_P}) \right) \right] \end{aligned} \quad (64)$$

in the latter part of the year ( $1/2 \leq \tilde{t} < 1$ ).

Figure 11 shows the time evolution of the skill for such a model, in the case of a spring start of for the case of a fall start. It is apparent that skill is lost more rapidly when the system is in the unstable spring state than when the model is in the stable fall state. This agrees with the role of the stability parameter  $c$  in controlling whether nearby trajectories converge or diverge, as explained previously.

A concept often noted in the literature on model skill is that of *reemergence*. In general, model skill is expected to decrease monotonically away from a given initial condition. However, some models exhibit a slight increase in skill following their initial decline; a feature referred to as reemergence. One hypothesis put forward to explain this phenomenon is that of natural variability. Initial work has suggested that the simple model may demonstrate a reemergence of skill at long time if forced periodically, which motivates further consideration of this concept in future work.

## 4 Application of Results to Global Climate Models

In practice, the seasonal prediction of Arctic sea ice is not done using simple one-dimensional models, but using high resolution Global Climate Models (GCMs). From a consideration of the origins of predictability in a simple model, however, it is evident that GCMs must be capable of capturing the important feedbacks at play in the Arctic (principally, the



Figure 11: The decrease in skill over time for different start months; one during the unstable season (spring;  $c = 0.1$ ) and one going into the stable season (fall;  $c = -2.0$ ).

positive ice-albedo feedback and the negative longwave stabilization feedback) if they hope to predict Arctic sea ice on a seasonal basis. It might be expected that if such feedbacks are incorporated in the GCMs, they will show the same seasonal variation in standard deviation seen in the satellite data and explained by the simple model considered above.

#### 4.1 CMIP5 data

To assess the success of GCMs at reproducing the seasonal cycle in the standard deviation sea ice anomaly trajectories that forms the basis of our understanding of predictability, data from the CMIP5 model ensemble is analysed. CMIP5 is the fifth Climate Model Inter-comparison Project, and gathers state of the art GCMs for a series of standardised runs with common forcings to enable comparison between the models. Available statistics include the ice thickness, the sea ice extent, and the ice volume. From the ice extent, a secondary metric known as the Equivalent Ice Extent (EIE) may be calculated, which is the area within the sea ice margin. This may be used to avoid biases resulting from the location of the ice in relation to land.

To analyse the GCM sea ice predictability, timeseries of the statistics listed above were taken from the CMIP5 historical runs. These runs start between 50 and 150 years before present, depending on the model, and are run through to the modern day with conditions mimicking those of the last century. For each model, the data was detrended, and its seasonal cycle was removed. The remaining timeseries anomalies were then split into years, with each year considered an independent anomaly trajectory. This enabled calculation of the annual cycle of the trajectory standard deviation, both for individual models and for the CMIP5 data as a whole, as shown in Figure 12 for the EIE.

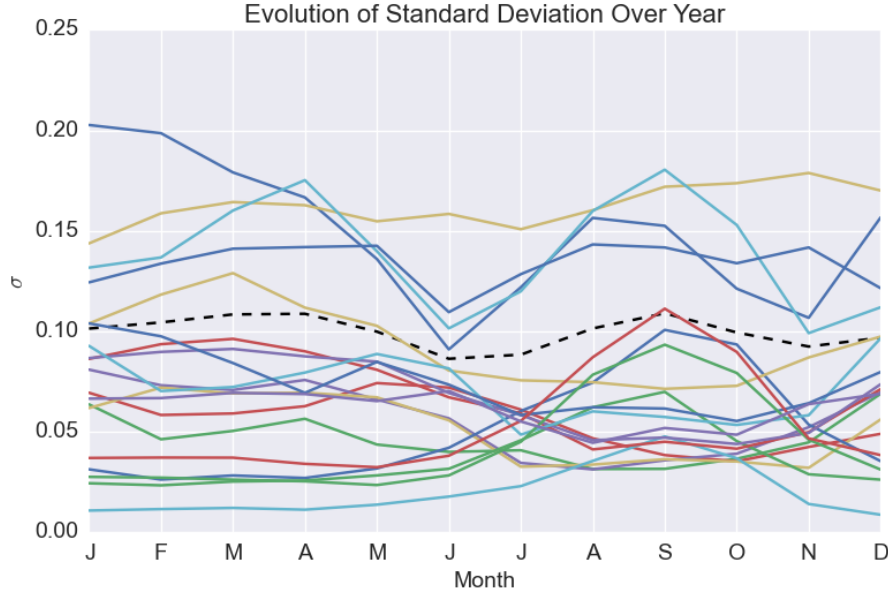


Figure 12: Annual evolution of the standard deviation of the EIE anomaly for the different models included in CMIP5, with the multimodel standard deviation shown as the black dashed line.

It is evident from Figure 12 that the models, in general, do not capture the seasonal cycle in the sea ice anomaly standard deviation seen in the satellite data. This is problematic given the relation of the seasonal variation in standard deviation to the annual cycle in feedback strengths, which is fundamental to the problem of seasonal prediction. Some insight can be gained into why the models might be failing by plotting the EIE before the seasonal cycle is removed (Figure 13). In Figure 13 it is seen that the models may be split into two rough categories; those that capture the naturally observed sinusoidal seasonal cycle in the Arctic sea ice, and those that have a somewhat unnatural cycloidal-shaped seasonal cycle. If the ice extent is considered instead of the EIE, however, this cycloidal behaviour is eliminated and all the models display a sinusoidal seasonal cycle. This suggests that the models may have been tuned to fit the ice extent rather than the EIE, resulting in the strange seasonal cycles seen in Figure 13, and a loss of the statistical behaviour pertinent to seasonal prediction.

It is hoped that the models might succeed better at reproducing the statistics of the ice thickness and ice volume, as these metrics are dominated by the less noisy multi-year ice, and consequently not as prone to the large interannual fluctuations experienced by the sea ice extent.

## 4.2 Ensemble size & statistic convergence

When using GCM runs to make statements about the Arctic sea ice, a further issue is that of ensemble size. Under the assumption of independence, the CMIP5 data might be thought of as providing a collection of stochastic trajectories of Arctic sea ice extent. How many

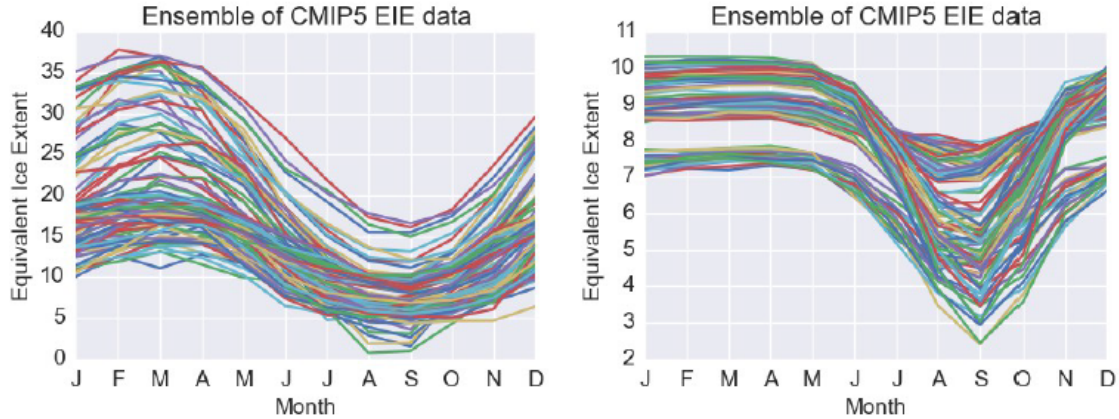


Figure 13: The seasonal cycle of Equivalent Ice Extent (EIE) for a selection trajectories from each of the CMIP5 models. Left: those models that capture a sinusoidal seasonal cycle, right: those models with a cycloidal seasonal cycle.

models then are needed to make robust statistical statements about the behaviour of ice, say under a forcing like that associated global warming?

In Figure 14, the simple model SDE is integrated for increasing ensemble sizes ranging from 10 to 1000, and the time evolution of the resultant standard deviation is compared to that computed from the analytic solution. Convergence occurs relatively quickly, with ensemble sizes of around 50 producing standard deviations that are in reasonable agreement with the analytic result. Even such a modest ensemble size is somewhat larger than the number of models included in CMIP5, though. This should be taken into consideration when drawing conclusions from GCM data derived from a limited number of runs.

## 5 Conclusions & Future Work

The application of stochastic perturbation theory to a simple model has allowed the annual variations in the predictability of Arctic sea ice to be traced back to the stability of the system, which arises from the presence of feedbacks. The dominance of the positive ice-albedo feedback in spring makes the system unstable, resulting in low predictability of the sea ice minimum going into summer. The negative longwave stabilization feedback in fall, however, focusses sea ice anomaly trajectories going into winter, increasing predictability during this period. It was seen that the problem of attribution works in reverse, with an unstable system making anomalies easy to attribute to events earlier in the season, and a stable system complicating attribution.

It was further shown that the system stability may be directly related to the concept on model skill. In the unstable regime (i.e. spring), model skill drops off faster than in the stable regime (i.e fall). This is likewise a consequence of trajectories diverging away from an initial condition when positive feedbacks dominate, and converging when negative feedbacks dominate. Change in the strength of the ice-albedo and longwave stabilization feedbacks under global warming would alter the stability properties of the system, affecting

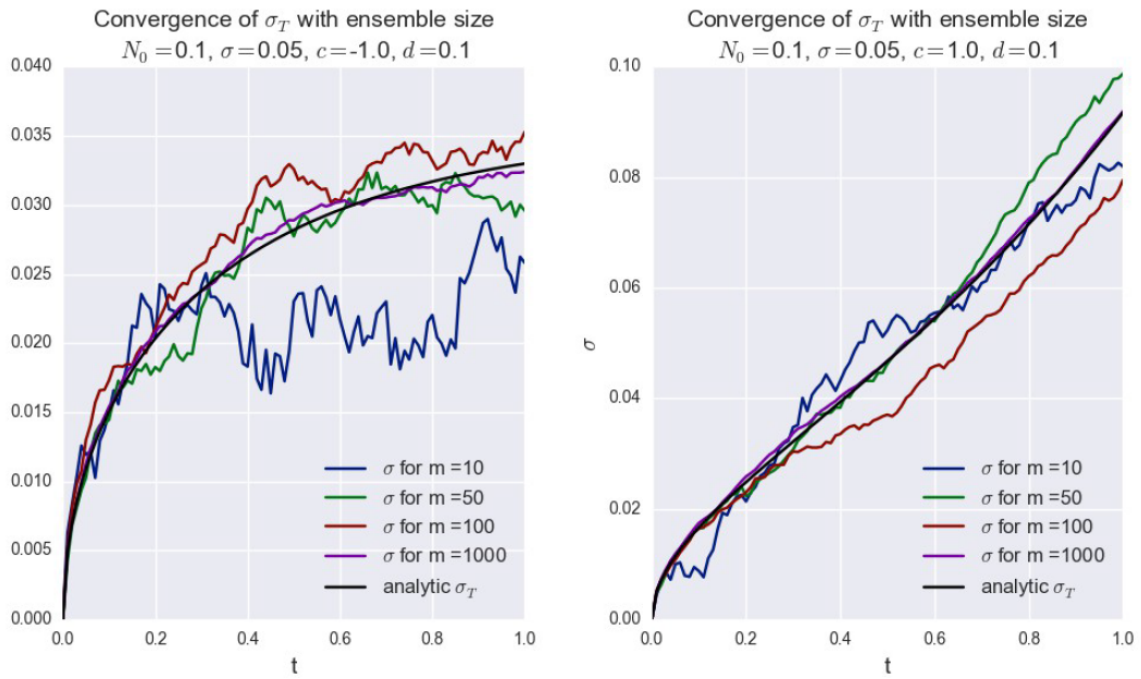


Figure 14: Convergence of the standard deviation from the numerical integration of ensembles to the analytically computed standard deviation when the system is in a stable regime (left) and an unstable regime (right).

our ability to predict the summer and winter sea ice extents.

A brief analysis of GCM data suggests that current generation models may experience difficulty in the seasonal prediction of Arctic sea ice as their failure to capture the annual cycle of sea ice variance suggests difficulty in reproducing principal physical feedbacks that underlie the evolution of sea ice anomalies.

It should be noted that the methodology presented in this project is by no means constrained to the Arctic sea ice system, but may in fact be applied to any problem for which there is relatively small magnitude noise superposed on a strong periodic cycle. As such, future work might focus on using this framework to consider other climate signals for which seasonal or interannual prediction is of interest.

## References

- [1] I. EISENMAN AND J. S. WETTLAUFER, *Nonlinear threshold behavior during the loss of Arctic sea ice*, Proceedings of the National Academy of Sciences of the United States of America, 106 (2009), pp. 28–32.
- [2] P. K. KLOEDEN AND E. PLATEN, *Numerical Solutions of Stochastic Differential Equations*, Springer-Verlag, Berlin, 2008.
- [3] G. A. MAYKUT AND N. UNTERSTEINER, *Some results from a time-dependent thermodynamic model of sea ice*, Journal of Geophysical Research, 76 (1971), pp. 1550–1575.
- [4] W. MOON AND J. S. WETTLAUFER, *On the existence of stable seasonally varying Arctic sea ice in simple models*, Journal of Geophysical Research, 117 (2012), p. C07007.
- [5] ———, *A stochastic perturbation theory for non-autonomous systems*, Journal of Mathematical Physics, 54 (2013), p. 123303.
- [6] D. SCHRÖDER, D. L. FELTHAM, D. FLOCCO, AND M. TSAMADOS, *September Arctic sea-ice minimum predicted by spring melt-pond fraction*, Nature Climate Change, 4 (2014), pp. 353–357.
- [7] J. ZHANG, R. LINDSAY, M. STEELE, AND A. SCHWEIGER, *What drove the dramatic retreat of arctic sea ice during summer 2007 ?*, 35 (2008), pp. 1–5.